Renewable Energy 143 (2019) 1397–1405

Contents lists available at ScienceDirect

Renewable Energy

journal homepage: www.elsevier.com/locate/renene

MWCNT-COOH supported PtSnNi electrocatalysts for direct ethanol fuel cells: Low Pt content, selectivity and chemical stability

Luanna S. Parreira [a, 1], Rodolfo M. Antoniassi [b, 1], Isabel C. Freitas [c, 2], Daniela C. de Oliveira [d], Estevam V. Spinacé [b], Pedro H.C. Camargo [c, 3], Mauro C. dos Santos [a, *]

[a] Universidade Federal do ABC (UFABC), Av. dos Estados, 5001, CEP 09210-580, Bangú, Santo André, SP, Brazil
[b] Instituto de Pesquisas Energéticas e Nucleares – IPEN-CNEN/SP, Av. Prof. Lineu Prestes, 2242, CEP 05508-000, Cidade Universitária, São Paulo, SP, Brazil
[c] Universidade de São Paulo (USP), Av. Prof. Lineu Prestes, 748, CEP 05508-000, Cidade Universitária, São Paulo, SP, Brazil
[d] Laboratório Nacional de Luz Síncroton (LNLS), R. Giuseppe Máximo Scolfaro, 10.000, CEP 13083-100, Polo II de Alta Tecnologia de Campinas, Campinas, SP, Brazil

ARTICLE INFO

Article history:
Received 27 March 2018
Received in revised form
14 May 2019
Accepted 16 May 2019
Available online 22 May 2019

Keywords:
DEFC
Multiwalled carbon nanotubes
PtSnNi
Products of reaction
Metal dissolution

ABSTRACT

PtSnNi electrocatalysts (60: 40: 40 mass ratio) supported on Vulcan® XC-72 (Cabot) carbon and COOH-functionalized multiwalled carbon nanotubes (Cheaptubes®) with 15% of metal loading were prepared. The nanoparticles size of 2–3 nm for both supports was estimated by HRTEM. In the direct ethanol fuel cell experiments, PtSnNi/C presents 50 mA cm^{-2} reaching the maximum power density (MPD) of 12 mW cm^{-2} and decreasing at higher currents, while PtSnNi/MWCNT-COOH obtains similar values of MPD (60 mA cm^{-2}), but keeping the best performance. By GC (gas chromatography) technique, it was possible to observe that the electrocatalyst supported on MWCNT-COOH favored the ethanol oxidation to acetaldehyde and acetic acid, although the material supported on Vulcan® XC-72 carbon presented almost 100% of selectivity for acetaldehyde. This behavior was maintained also when the current of 0.1 A was applied for 80 min. For the PtSnNi/C electrocatalyst, the selectivity to only acetaldehyde can be related to Sn and Ni dissolution process that can become the electrocatalytic activity similar to Pt/C, decreasing the power density as observed in our experiments. Established by EDS analysis, after 80 min of polarization, the Ni and Sn relative atomic ratio was lower on the catalytic anodic layer of PtSnNi/C than on PtSnNi/MWCNT-COOH.

1. Introduction

The important challenges for fuel cells technology are related to the reduction of Pt loading on the electrocatalysts and increase the stability of the materials under operation conditions [1,2]. Pt-based electrocatalysts are mostly used due to its (electro)chemical stability and favorable adsorption of organic molecules on its surface, facilitating the small organic molecules oxidation [3,4]. However, the wide and efficient fuel cells application as an alternative technology of clean energy conversion is limited because Pt is a rare and expensive metal (approximately USD 27400.00 per Kg [5]). Moreover, its activity is impaired by irreversible CO poisoning on its surface [6], an intermediate produced from the small organic molecules (SOM) oxidation reaction such as methanol and ethanol.

Research on the direct application of these alcohols in fuel cells aims to develop electrocatalysts [7,8] that use Pt auxiliary metals to reduce costs while increasing activities. Moreover, it is desired that these multimetallic materials allow the oxidation reaction of alcohols at potentials less positive than on Pt pure one, decreasing the intensity of poisoning by oxidation of intermediates such as CO [9,10] on its surface and optimizing the electrocatalytic performance [11]. In the case of ethanol, the C–C [12] bond cleavage is aimed to forestall the formation of acetic acid, which is inefficiently oxidized by the known materials so far.

* Corresponding author.
E-mail address: mauro.santos@ufabc.edu.br (M.C. dos Santos).
[1] Universidade Federal do ABC (UFABC), Av. dos Estados, 5001, CEP 09210-580, Bangú, Santo André - SP, Brazil.
[2] Department of Heterogeneous Catalysis, Max-Planck-Institut für Kohlenforschung, Kaiser-Wilhelm-Platz 1, Mülheim an der Ruhr, D-45470, Germany.
[3] Department of Chemistry, University of Helsinki, A.I. Virtasen aukio 1, Helsinki, Finland.

https://doi.org/10.1016/j.renene.2019.05.067
0960-1481/

For the ethanol oxidation, Sn [13,14] is often employed as an auxiliary metal to Pt in the electrocatalyst since it affects the adsorption and dissociation processes of ethanol molecules, contributing to inducing the cleavage of C–C bond with greater selectivity than the observed on pure Pt [15]. This effect is strongly linked to the amount and distribution of Sn on the electrocatalyst as well as the nanostructure preparation method [16,17]. Additionally, binary and ternary alloys also have been developed in order to oxidize the intermediate species on Pt surface and reduce its poisoning. However, the role of the third metal is not well established and deserve further investigations [18–24].

It has been established that Ni also can be an auxiliary metal to Pt for the ethanol oxidation electrocatalysis [25–27]. It is suggested that the presence of nickel oxides modify the Pt electronic properties performing the ethanol oxidation by both electronic effects and bifunctional mechanism [28]. This leads to the weakening the CO adsorption on Pt surface and improvements in its electrocatalytic activity and stability. In addition, the Ni in conjunction with Sn can facilitate the C–C bond cleavage and can promote the adsorbed CO desorption on Pt surface by water-gas shift reaction, increasing the selectivity for hydrogen production, as indicated by Huber and collaborators [29].

Regarding the effect of the support, carbon is mostly used in electrocatalysts for small organic molecules oxidation reactions [30]. This structure presents high surface area, porous structure and good conductivity, but is not electrocatalytic for EOR [31]. Furthermore, research indicates that Pt is able to catalyse the degradation of carbon [32]. Aiming to improve the electrocatalyst activity, it has been shown that carbon nanotubes and nanoribbons [33–36], when used as a support, can increase the electroactivity of the materials due its electric conductivity as good or better than the graphite carbon [37]. Multiwalled carbon nanotubes have several applications due to its unique structural characteristics, electronic properties, electrochemical stability and thermal conductivity [38], being also more resistant to corrosion process than amorphous carbon [39]. On the other hand, its hydrophobic and inert surface hinders the metal nanoparticles anchorage, being developed functionalization methods [40] that incorporate N and O atoms by surface defects with the goal to intensify the affinity between support and metals [41], contributing to the electrocatalytic activity of the material.

In a study performed by Shao et al. [42], Pt/CNT presented a rate degradation twice lower than Pt/C under same conditions of accelerated stress tests, that was attributed to a specific interaction between Pt - functionalized support and to the carbon nanotubes greater resistance to electrochemical oxidation.

Previously, Parreira et al. [43] studied PtNi/C and PtSnNi/C electrocatalysts for ethanol oxidation reaction and observed that after 1000 cyclic voltammetries, Ni presented lower dissolution from ternary than binary material. Additional to this result, it was possible to see, for the PtSnNi/C, a change in the formation of the products after cycling. Before accelerated stress test (AST), acetaldehyde and acetic acid were the main products while after 1000 cycles the acetaldehyde was detected only.

Herein, we describe a comparison in terms of DEFC performance for PtSnNi (nominal metal mass ratio of 60:40:40) electrocatalysts supported on amorphous carbon black (Vulcan® XC-72) and multiwalled carbon nanotubes (Cheaptubes®) in order to unravel the effect of the support and trimetallic compositions. The formation of products was monitored by GC technique, and our results demonstrated that the support and chemical composition strongly affected the performance of the produced electrocatalysts in terms of power density and stability.

2. Experimental section

2.1. Reagents

$H_2PtCl_6 \cdot 7H_2O$ (8% in H_2O, Sigma-Aldrich®), $SnCl_2 \cdot H_2O$ (reagent grade, 98%, Sigma-Aldrich®), $NiCl_2 \cdot 6H_2O$ (PA, Synth®), Citric acid (ACS reagent, ≥99.5%, Sigma-Aldrich®), Ethylene glycol (PA, Synth®), Vulcan® XC-72 carbon (Cabot) and –COOH functionalized multiwalled carbon nanotubes (99%, Cheaptubes®). All reagents were used as received.

2.2. Preparation of the electrocatalysts

The nanoparticle electrocatalysts were prepared by an adapted protocol described elsewhere [39]. Typically, the precursor resin was formed by dissolving citric acid in ethylene glycol at 60 °C, followed by the addition of metal precursor reagents ($PtCl_6^{2-}{}_{(aq)}$, $Sn^{2+}{}_{(aq)}$, and $Ni^{2+}{}_{(aq)}$) to obtain electrocatalysts Pt:Sn:Ni with mass ratio 60:40:40 and stirred during 45 min. The metal/citric acid/ethylene glycol molar ratio corresponded to 1:50:200. The precursor resin was mixed with high surface area Vulcan® XC-72 carbon or functionalized MWCNT-COOH to obtain electrocatalysts with a metal loading of 15 % wt. The resulting mixture was homogenized in an ultrasonic bath and thermally treated under an ultrapure N_2 atmosphere for 3 h at 400 °C with a heating rate of 5 °C min^{-1}.

2.3. Physicochemical characterization

X-ray diffraction (XRD) was performed using a Bruker Focus diffractometer with a CuKα radiation (λ = 0.1540 nm) source that was operated in continuous scan mode (2° min^{-1}) from 20° to 80° (2θ degrees) to determine the crystalline phases and to estimate the mean crystallite size and the lattice parameter. High-resolution transmission electron microscopy (HRTEM) analyses were performed using a high-resolution JEOL microscope JEM 2100 operating at 300 kV to observe the morphology of the particles and to measure their sizes. All the samples for the HRTEM analysis were prepared ultrasonically dispersing the catalyst particles in a formaldehyde solution. Drops of the suspension were deposited onto a standard Cu grid covered with a carbon film. The average particles size was determined using the Image J software package, and more than 250 different particles were analysed. Energy dispersive spectroscopy (EDS) using a scanning electron microscope (FESEM JSM – 6701F JEOL) operating at 20 kV was used to measure the chemical composition of the PtSnNi and PtSn commercial electrocatalysts before and after DEFC tests. X-ray photoelectron spectroscopy (XPS) analysis was performed with a SPECSLAB II (Phoibos-Hsa 3500 150, 9 channeltrons) SPECS spectrometer, with Al Kα source (E = 1486.6 eV) working at 15 kV, Epass = 40 eV, 0.2 eV energy step and 1 s per point was the acquisition time. The synthesized electrocatalysts were kept on stainless steel sample-holders and transported under an inert atmosphere to the pre-chamber of the XPS staying there in a vacuum atmosphere for 2 h. The residual pressure inside the analysis chamber was ~1×10^{-9} Torr. The binding energies (BE) of the Pt 4f, Sn 3d, Ni 2p and O 1s spectral peaks were referenced to C 1s peak, at 284.5 eV, providing accuracy within ±0.2 eV.

2.4. Evaluation of fuel cell performance

The performance for the electrocatalysts was measured in a single cell with a geometric area of 5 cm^2. For the membrane electrode assemblies, the electrocatalytic films were deposited on the gas diffusion electrodes (carbon cloth Teflon treated – EC-CC1-

060T, ElectroChem, Inc.) from a homogeneous ink made with Nafion® solution (5 wt %, Aldrich®) and isopropanol (P.A, Synth ®). PtSnNi/C, PtSnNi/MWCNT-COOH and the commercial PtSn/C E-TEK (20 wt %) commercial - for comparison - were used as anodes with total metal loading (0.5 $mg_{Pt}cm^{-2}$) on carbon cloth gas diffusion electrode, while Pt/C E-TEK (20 wt %) as the cathode (1 mg cm^{-2} of metal).

The electrodes were hot pressed on both sides of a Nafion®115 membrane at 125 °C for 3 min under a pressure of 247 kgf cm^{-2}. Prior to use, the membranes were exposed to 3 wt % H_2O_2 washed thoroughly with distilled water and treated with 0.5 mol L^{-1} H_2SO_4. The temperature was set to 100 °C for the unit cell and 80 °C for the oxygen humidifier. The ethanol (2 mol L^{-1}) was delivered at approximately 2 mL min^{-1}, and the oxygen flow was set to 500 mL min^{-1} with 2 bar of pressurization. Polarization curves were obtained using a TDI RBL 488 electronic load connect to unit DEFC device.

Before the tests, H_2 was used in the unit cell at 500 mV of applied potential during 2 h to remove the impurities from electrocatalysts preparation and deposition on electrodes and to activate the Nafion®115 membranes. Hence, the ethanol solution was inserted into the system to obtain the polarization curves when the open circuit voltage was kept stable. Considering the same metal loading on the electrodes (0.5 $mg_{Pt}cm^{-2}$), both current and electrical power obtained from the experiments were normalized by electrode area (5 cm^2) and presented as current density j ($mA{\cdot}cm^{-2}$) and power density ($mW{\cdot}cm^{-2}$). The polarization curves were collected in the potential range from open circuit to minimum voltage values.

Gas Chromatography (GC) was used to identify the ethanol electrooxidation products using a 7890A Agilent GC System. For this study, the operational parameters were defined as capillary column Plot-U (30 m of length and 0.53 mm of diameter); thermal conductivity detector (TCD) using hydrogen gas at a flow rate of 45 mL min^{-1}; sample splitting at inlet (SPLIT Mode) 1/20; injected sample volume of 1 μL. The operating temperatures were: inlet at 180 °C, detector at 200 °C and column starting at 60 °C for 2 min and increasing 20 °C min^{-1} until 160 °C. All the collected anodic aliquotes were cooled in an ice bath at a constant current for monitoring of the reaction products concentrations until values close to the minimum voltage (during 80 min) following the same protocol used by Antoniassi et al. [44].

The injections were performed manually and the elution times ranged from ca. 0.70 min for CO_2 to ca. 8.45 min for acetic acid, with excellent peak separation. Ethanol and the formed products such as acetaldehyde, ethyl acetate and acetic acid were quantified using a calibration curve (Fig. S1). The ethanol electrooxidation products determined from anodic effluent were analysed with respect to selectivity (S_p) by equation (1).

$$\% S_p = \frac{C_p}{C_{PT}} x\ 100\% \quad (1)$$

where C_p is the concentration of a specific reaction product (C_{AAL} = Acetaldehyde e C_{AA} = Acetic Acid and C_{PT} is the total concentration of formed products. Ethyl acetate, when determined, was converted to acetaldehyde and acetic acid.

3. Results and discussion

3.1. Characterization of the electrocatalysts

Fig. 1 shows SEM (Fig. 1A and D) and HRTEM images (Fig. 1B and E) for the PtSnNi NPs supported on Vulcan® XC-72 carbon (Fig. 1A and B) and on MWCNT-COOH (Fig. 1D and E). Fig. 1C and F depict the corresponding histograms of size distribution obtained from (Fig. 1B and E), respectively. The SEM images reveal the granular and tubular morphologies of the Vulcan® XC-72 carbon and MWCNT-COOH supports (Fig. 1A and D, respectively). The particle size for the Vulcan® XC-72 carbon support corresponded to about 40 nm in diameter, while the MWCNTs were 15 nm in diameter and presented a wall thickness of 4 nm (Fig. S2). HRTEM images indicate that the PtSnNi NPs were uniformly dispersed at the surface of both supports. They displayed relatively monodisperse sizes and no significant agglomeration at the surface of the support took place. The histograms of size distribution suggest that the PtSnNi NPs sizes corresponded to 2.7 ± 0.8 and 1.9 ± 0.3 nm in the PtSnNi/C and PtSnNi/MWCNT-COOH materials, respectively. The smaller NPs size for the MWCNTs sample may be related to the presence of surface COOH, which could provide more sites for NPs nucleation and subsequent growth during the synthesis. It is plausible that this increased number of nucleation sites, under the same concentration of metal precursors, lead to a decrease in the final diameter of the obtained NPs [45] and possibly to a low standard deviation for average size, as also seen by Li et al. [46].

The PtSnNi/C, PtSnNi/MWCNT-COOH and PtSn/C E-TEK electrocatalysts surface composition and oxidation states of the components are investigated by XPS. The fitting curves and deconvoluted spectra of Pt 4f, Sn 3d and Ni 2p peaks for the corresponding electrocatalysts are shown in Fig. 2A–C while in Fig. 3 the C 1s and O 1s peaks are presented. The corresponding XPS parameters for C 1s are summarized in Table 1. As can be seen in Fig. 2A, the Pt 4f core level region was deconvoluted using three components for all electrocatalysts. The first $4f_{7/2}$ component with low binding energy, at 71.7–71.4 eV, can be attributed to metallic Pt coming from the PtSn alloy. The second one, located at 72.6–73.2 eV, could be assigned to Pt^{2+} (PtO and $Pt(OH)_2$-like surface species). The third component, which had higher binding energy (74.4–74.1 eV), corresponded to Pt^{4+}. According to the literature, the binding energies values of Pt $4f_{7/2}$ levels for the three oxidation states are reported as follow: Pt^0 71.0 eV, Pt^{2+} 72.8 eV and Pt^{4+} 74.3 eV [47]. The slight shift toward higher values of binding energy with respect to the literature is attributed to the strong metal-support interaction and to the ultrasmall size of Pt nanoparticles [44,48,49]. It is known that as the size of Pt particles decreases, the Pt 4f core level peak in XPS spectra shifts to the higher binding energy [48]. This is expected in 2–3 nm nanoparticles, in agreement with the HRTEM results.

Fig. 2B shows the XPS spectra of Sn $3d_{5/2}$ core level for PtSnNi/C, PtSnNi/MWCNT-COOH, and PtSn/C E-TEK electrocatalysts. The Sn $3d_{5/2}$ peaks were adjusted with only one component located at 487.1–486.7 eV that could be ascribed to SnO_x, in which oxygen is chemisorbed. SnO_2 and SnO have a very small binding energy difference, so it is difficult to distinguish between these two species. According to the literature [47,50], the position of Sn^0 that is alloyed to a metal with different electronegativity could shift the signal towards higher binding energy values. Considering 1.8 eV the highest shift reported [51,52], this value is close to the position of 487.1–486.7 eV that we have attributed as SnO_x. The Sn^0 species may be present in this electrocatalysts as PtSn alloy. In this work, the PtSn/C and PtSnNi/C electrocatalysts could present a small contribution of this reduced species in the peak attributed to SnOx and for PtSnNi/MWCNT-COOH a major contribution, that is why the Sn $3d_{5/2}$ peak of PtSnNi/MWCNT-COOH shown an asymmetric shape. This result can be corroborated by XRD analysis (Fig. S3), where PtSnNi/MWCNT-COOH presented diffraction peaks close to 33° and 52° assigned to (101) and (211) planes of SnO_2 cassiterite phase (JCPDF 411445) with a slight shift to 2θ lower values when compared to Pt (JCPDF 040802). This indicates a partial insertion of Sn into Pt structure extending its lattice parameter to 3.952 nm. On

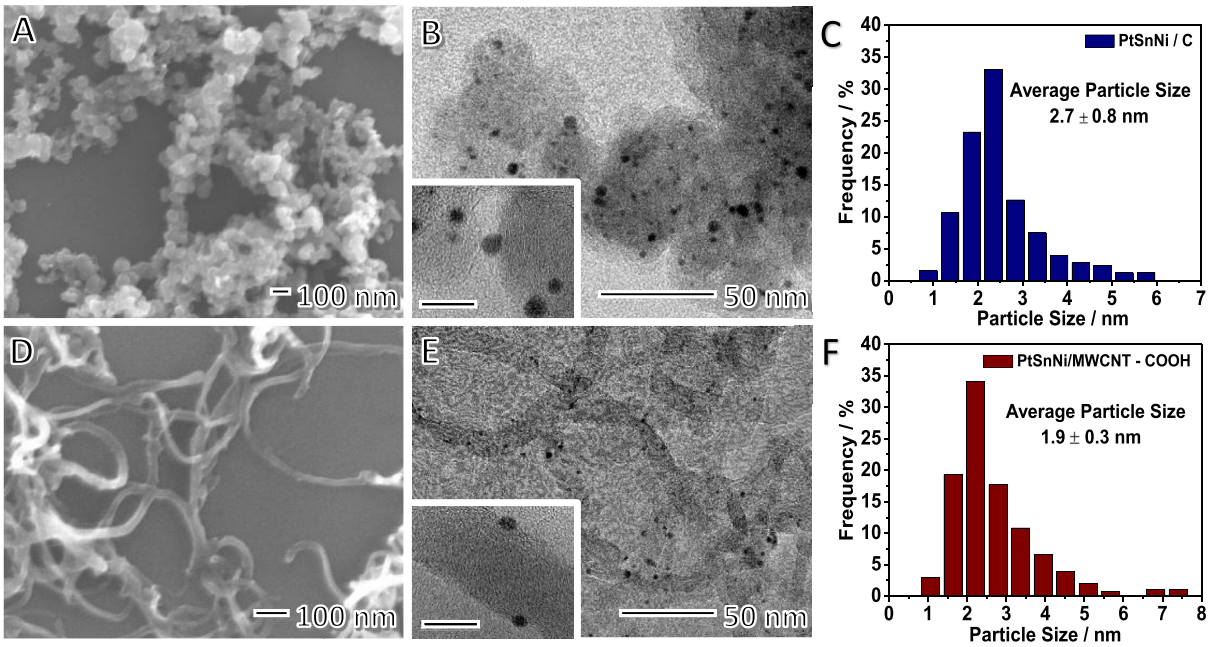

Fig. 1. SEM (A and D) and HRTEM (B and E) images for PtSnNi/C (A and B) and PtSnNi/MWCNT-COOH (D and E) electrocatalysts. The scale bars in the inset correspond to 10 nm. (C) and (F) show the histograms of size distribution obtained from (B) and (E), respectively.

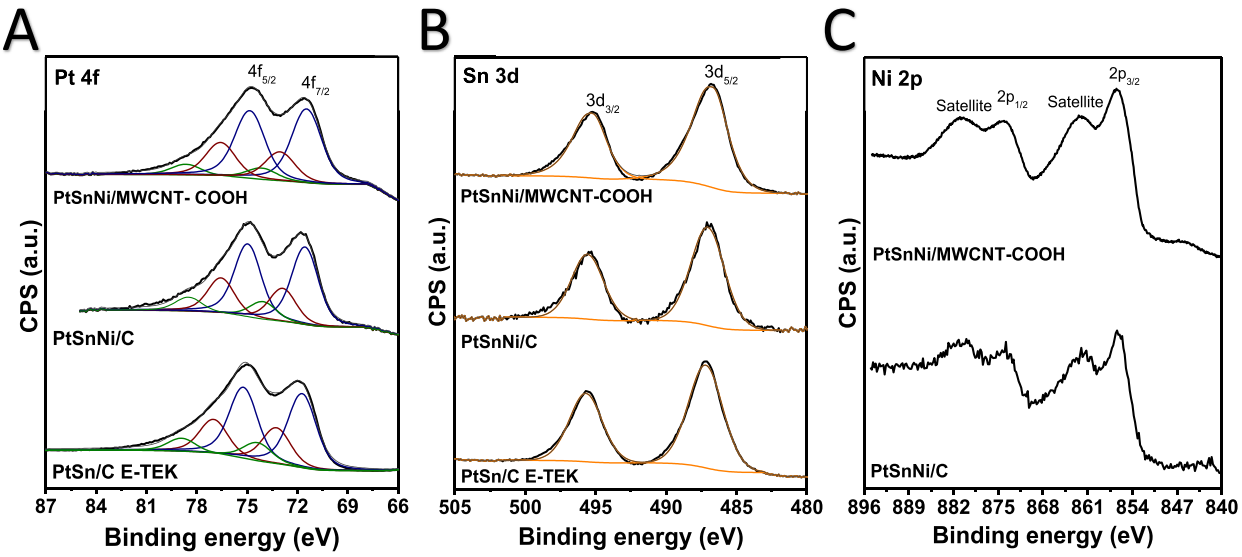

Fig. 2. XPS spectra of the Pt 4f (A), Sn 3d (B), and Ni 2p (C) core-levels for the PtSnNi/MWCNT-COOH, PtSnNi/C, and commercial PtSn/C E-TEK catalysts.

the other hand, there are no peaks from Sn oxide species in the PtSnNi/C diffractogram. This material presented a lattice parameter of 3.918 nm. It is indicated that Sn and Ni contribute to the Pt structure in different ways: while Ni leads to a contraction in the lattice parameter, Sn leads to expansion. This fact explains the obtained lattice parameter for the ternary electrocatalyst supported on Vulcan® XC-72 carbon being very close to Pt/C (3.911 nm) [53,54] one.

The Ni 2p spectra showed a complex structure because of multielectron excitation (shake-up peaks) which leads to intense satellite signals (Fig. 2C) of high binding energy adjacent to the main peak [55–57]. After considering the shake-up peaks, the Ni $2p_{3/2}$ peak located at 856.5–856.2 eV could be ascribed to the presence of $Ni(OH)_2$. The presence of the oxidized Ni species can help to decrease the corrosion effects in the electrocatalysts during the application, mainly to PtSnNi/MWCNT-COOH that presented the highest concentration of these species on its surface, probably due to the presence of segregated Ni.

Regarding the C 1s spectrum (Fig. 3A), it can be deconvoluted into six peaks. The C 1s at 284.5 eV was considered the reference level of calibration. The lowest binding energy and dominant peak at about 284.5 eV corresponds to graphitic carbon phase, followed by the peak at around 286.0 eV assigned to hydrocarbons (C–H) from defects on the graphitic structure. It can also be observed the

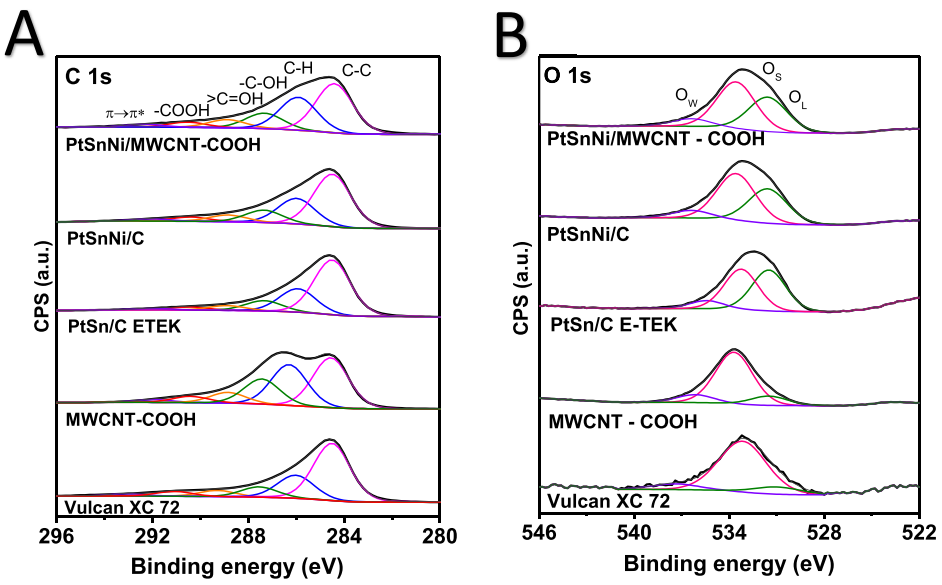

Fig. 3. XPS spectra for the C 1s (A) and O 1s (B) core-levels for the PtSnNi/MWCNT-COOH, PtSnNi/C and commercial PtSn/C E-TEK electrocatalysts compared to their respective supports.

Table 1
XPS characteristics of C 1s region for pure carbonaceous supports, PtSn/C E-TEK and PtSnNi prepared samples.

Electrocatalyst	Binding energy C 1s (eV)						Peak intensity (%)
	Peak I C–C	Peak II C–H (defects)	Peak III –C–OH	Peak IV > C=O	Peak V -COOH	Peak VI π→π[a]	I_{Oxy}/I_C[b]
Vulcan XC-72	284.5 (57)[a]	286.0 (21)	287.5 (10)	289.2 (6)	290.8 (4)	292.8 (2)	19
MWCNT-COOH	284.5 (37)	286.0 (30)	287.4 (19)	288.8 (8)	290.4 (4)	291.9 (2)	46
PtSn/C E-TEK	284.5 (55)	285.9 (24)	287.3 (11)	289.0 (5)	290.4 (3)	291.9 (2)	23
PtSnNi/C	284.5 (51)	285.9 (25)	287.3 (12)	288.8 (6)	290.4 (4)	292.0 (2)	24
PtSnNi/MWCNT-COOH	284.5 (43)	285.9 (29)	287.3 (14)	288.8 (7)	290.5 (5)	292.3 (2)	34

[a] Percent of species.
[b] Intensity of three oxygen-containing functional groups (peaks III–V) in % of total C 1s area.

three carbon-oxygen bonding structures for the –C-OH, >C=O and –COOH at approximately 287.5, 289.2 and 290.8 eV, respectively. The subpeak located at higher than 292.8 eV is related to π → π* plasmon excitation (Table 1). It was observed that the contribution of carbon oxygenated species for PtSnNi/MWCNT-COOH is higher than for the ternary material supported on Vulcan® XC-72, even after the thermal treatment, but decreases probably due to the consumption of the oxygenated functional groups by particles anchorage/reduction process [58], as observed in a previous work [59].

The XPS of the O 1s core level for electrocatalysts is shown in Fig. 3B. The broad O 1s peak was deconvoluted in three components. According to the literature [60], the first component (O_I) centered at 531 eV was attributed to the lattice oxygen in the oxides. The second and dominant component (O_{II}) located at 533 eV was attributed to chemisorbed oxygen species (*e.g.*, OH^-) and functional C–O groups. The last component (O_{III}), with BE around 536 eV, was characteristic of adsorbed water and oxygen-containing carbon-functional groups.

The surface atomic ratio for Pt, Sn and Ni of electrocatalysts obtained from the XPS spectra are given in Table S1. The commercial material PtSn/C E-TEK presented a surface rich in Sn as observed in other studies [52,61,62] - probably due to its affinity for oxygen causing the Sn migration of the bulk electrocatalyst towards the surface [63] - as well the PtSnNi/C electrocatalyst, which also is supported on Vulcan® carbon. For the PtSnNi/MWCNT-COOH the Sn is slightly enriched while it is observed a significant Ni enrichment on the surface as compared to nominal bulk values, differently to works in the literature that use high Pt atomic ratio [49,52,62]. However, the ternary materials have a higher Ni metal atomic ratio than a commercial one and, in the case of MWCNT-COOH support, residual Ni from catalytic growth of carbon nanotubes [64] could be detected from the superior metal percentages after Ni anchorage process by the preparation method of the electrocatalysts.

3.2. DEFC experiments

After the activation step using hydrogen, ethanol (2 mol L^{-1}) was inserted into a unit cell with a flow of 2 mL min^{-1}. The temperature was increased to 100 °C and the oxygen was pressurized at 2 bar. The polarization curves were obtained after the open circuit voltage (OCV) stabilization and they are presented in Fig. 4A. The OCV for ethanol oxidation using both prepared PtSnNi materials was 0.65 V while for PtSn/C E-TEK the OCV was 0.64 V. For the to PtSnNi/MWCNT-COOH material, it is possible to observe from the polarization curve in Fig. 4A a voltage drop more pronounced in the activation region until around 15 mA cm^{-2}, where the electron transfer is limited by reaction activation energy and depends on the interaction between electrode and fuel molecule. However, for the

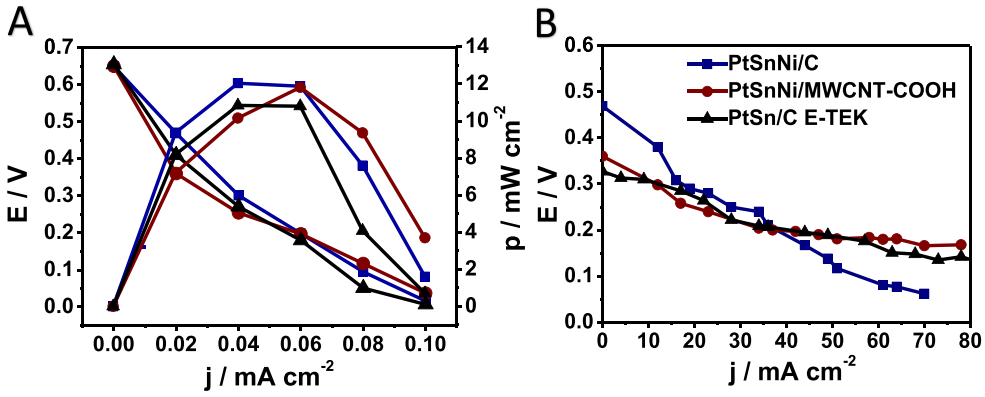

Fig. 4. (A) Polarization and power density curves in 5 cm^2 DEFC at 100 °C using PtSnNi/C, PtSnNi/MWCNT-COOH, and PtSn/C E-TEK (blue square, red cycle and black triangle traces, respectively) as the anode electrocatalysts (2 mg_{metal} cm^{-2}) and 20 wt% Pt/C E-TEK as the cathode catalyst (2 mg_{metal} cm^{-2}). Nafion® 115 was used as the membrane. The ethanol solution (2 mol L^{-1}) flow was 2 mL s^{-1}. O_2 pressurization = 2 bar. PtSn/C E-TEK (20% wt.) was used as anode for comparison. (B) Polarization curves at i = 0.1 A during 80 min. (For interpretation of the references to colour in this figure legend, the reader is referred to the Web version of this article.)

electrocatalyst supported on Vulcan® XC − 72 carbon, the voltage drop in this region was less pronounced, indicating that the electron transfer can occur more easily on this surface. Thus, PtSnNi/C maintained a better electrical performance until 50 mA cm^{-2} leading to about 12 mW cm^{-2} of maximum power density and decreasing soon after. The PtSnNi/MWCNT-COOH yielded the same maximum power density (also 12 mW cm^{-2}) with a current density of 60 mA cm^{-2}. These values were slightly higher than that obtained by PtSnNi/C, but keeping the best performance until both electrocatalysts reached their minimum potential value. Additionally, the ethanol oxidation using PtSnNi/C electrocatalyst presents a voltage drop by ohmic resistance slightly higher than using PtSnNi/MWCNT-COOH. On the other hand, from 60 $mAcm^{-2}$, the curve decreasing keeps between ohmic and mass transportation (diffusion) region, becoming the voltage values, and consequently, the power density values lower than those ones presented by PtSnNi/C.

Ribandeneira and coworkers [65], studied PtSnNi/C electrocatalysts in 75:15:10 and 75:10:15 atomic ratios, 20% of metal loading on Vulcan® XC-72 carbon, prepared using the reduction method by ethylene glycol. The operating conditions were: electrode with 1 mg_{Pt} cm^{-2}, ethanol 1 mol L^{-1} (flow rate 2 mL min^{-1}), 80 °C of temperature, an oxygen flow of 20 mL min^{-1} and 15 psi pressurization. Under these conditions, they obtained for the materials PtSnNi/C (75:15:10) an open circuit voltage 0.48 V and a maximum current density of 37 mA cm^{-2} in a maximum power density of 3 mW cm^{-2}. Using PtSnNi/C (75:10:15) electrocatalysts, it was observed an open circuit voltage of 0.45 V and a maximum current density of 23 mA cm^{-2} in a maximum power density of 2 mW cm^{-2}. The addition of Ni electrocatalyst doubled the power density obtained by the PtSn binary electrocatalyst prepared by the same method. In another study, Beyhan et al. [52] studied electrocatalysts PtSnNi/C (atomic ratio 80:10:10 and metal loading of 40% on carbon) prepared by the Bönnemann method for a DEFC using 2 mg of metal per cm^2 of electrode (and Nafion® 117 membrane) under the conditions: T = 80 °C, ethanol 1 mol L^{-1} (pressure = 1 bar) and O_2 pressurization of 3 bar. The OCV for ethanol was 0.75 V and the cell performance with the electrocatalyst was 30 $mWcm^{-2}$ at a current density of 120 $mAcm^{-2}$. Finally, Almeida et al. [66] have prepared a set of metal electrodes and analysed their performance in DEFC using 2 mg of Pt per cm^2 (Nafion® 117 membrane) under the conditions: T = 80 °C, ethanol 2 mol L^{-1} (pressure = 1 bar) and 3 bar of O_2 pressurization. For PtSnNi (79:19:02) electrocatalyst the open circuit voltage for ethanol was 0.72 V and electrical performance with 40 $mWcm^{-2}$ at a current density of 250 $mAcm^{-2}$.

It is noteworthy that the electrocatalysts between 75% and 80% of Pt in terms of atomic composition, compared to only approximately 33% of Pt (atomic percentage) in the materials described herein. In addition, the atomic ratio of Ni in the electrocatalyst bulk corresponded to around 45%, while in the literature is around 10%. Considering the metal atomic ratio and the metal loading on the support, the electrocatalytic layer used on anode side for this study is thicker than the ones presented by the works cited and summarized in the Table S2 and for the commercial PtSn/C E-TEK (20 wt %.) used for comparison. The catalytic layer thickening can increase the concentration polarization across the electrodes difficulting the measuring intrinsic catalyst properties [67]. In addition, it can be observed higher activation and ohmic losses when compared to high Pt/C ratio electrocatalysts [68] motivating studies about several methods of coating in MEAs using low-Pt-loading electrocatalysts [69,70]. Even being more indicated thin catalyst layers, the materials used in this work obtained results comparable to literature as seen in Table S2. Where the best PtSnNi electrocatalysts presented a mass power density of 30 W g_{Pt}^{-1} (using an anode with 2$mg_{Pt}cm^{-2}$) while our nanomaterials reached to 24 W g_{Pt}^{-1} but with an anode electrode containing only 0.5 $mg_{Pt}cm^{-2}$.

The electrical performance of the DEFC is related, among other factors, with the formation of the reaction products during the oxidation of the fuel at the anode of the cell. Thus, the anode effluent aliquots were collected at maximum current and power densities and analysed by GC (Fig. S4). It was observed the detection of CO_2, acetaldehyde (CH_3CHO), ethyl acetate ($CH_3COO{-}C_2H_5$) and acetic acid (CH_3COOH). The ethyl acetate can appear due to an esterification reaction between ethanol and acetic acid on the catalytic layer containing $-SO_3H$, from Nafion®. However, CO_2 and ethyl acetate were not identified for both electrocatalysts, and the acetic acid concentration was above to quantification limit of TCD for PtSnNi/C electrocatalyst. From information about the spectrum area and calibration curve previously plotted (Fig. S1), the concentrations of reaction products present in the effluents were calculated to obtain the selectivity relations. It was possible to observe that the electrocatalyst supported on MWCNT-COOH favored the ethanol oxidation to acetic acid and acetaldehyde, with higher selectivity for the last one. Furthermore, the material supported on Vulcan® XC- 72 carbon presented almost 100% of selectivity for acetaldehyde formation. Taking into account the low Pt loading and the relative high ethanol concentration used in the unit cell (2 mol L^{-1}) would not be expected for PtSn-based

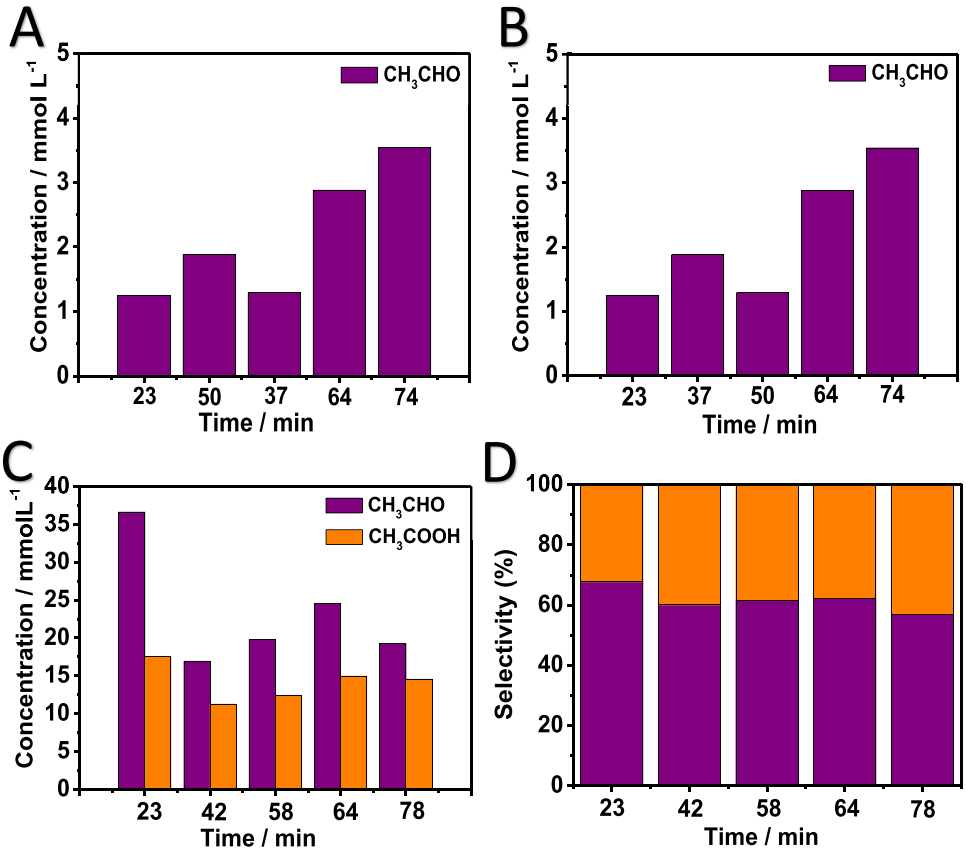

Fig. 5. Concentration of the ethanol (2 mol L^{-1}) oxidation reaction products in the DEFC anodic effluent at polarization of 0.1 A during 80 min (A) PtSn/C E-TEK, (B) PtSnNi/C, and (C) PtSnNi/MWCNT. (D) Bar graph depicting the selectivity of the PtSnNi/MWCNT material calculated from (C).

electrocatalysts the significantly CO_2 production [71]. Moreover, electrochemical measurements using Pt-based for ethanol oxidation reaction concluded that the CO_2 production reduced as ethanol concentration increase [72,73].

After obtaining the polarization curves, a current of 0.1 A was applied for 80 min. The electrical behavior and the product formation during the test period were observed. The results are presented in Fig. 4, where PtSnNi/C presents a voltage decreasing more intense than PtSnNi/MWCNT-COOH. This result can be related to greater carbon nanotubes stability [74] under operating conditions as well as the reaction products during the polarization.

Considering the data obtained by GC and displayed in Fig. 5, it is possible to observe that there was no relevant change in the formation of products from the fuel cell for 80 min. Using the PtSnNi/C electrocatalyst, the formation of acetaldehyde presents a slight increase, but that can be considered constant due to the concentration (about 3 mmolL^{-1}) and results from the dissolution process or poisoning of the electrocatalyst, jeopardizing the oxidation capability of its surface. For PtSnNi/MWCNT-COOH, the acetaldehyde concentration tends to increase with a decreasing of acetic acid during the polarization experiment. However, the selectivity for the product formation practically kept constant, which can justify the polarization curve behavior with a soft decay when compared to the one presented by electrocatalyst supported on multiwalled carbon nanotubes.

Almeida et al. [75] prepared three different compositions of PtSnNi/C electrocatalysts by thermal decomposition of polymeric precursor and determined, by high-performance liquid

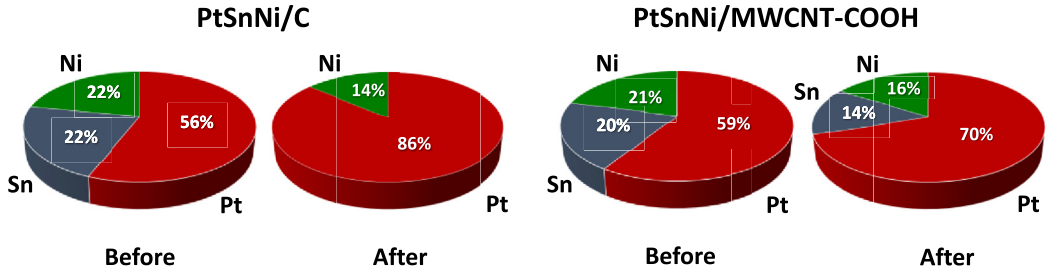

Fig. 6. Relative mass chemical composition of PtSnNi electrocatalysts determined by EDS before and after DEFC tests: Pt (red), Sn (blue) and Ni (green). (For interpretation of the references to colour in this figure legend, the reader is referred to the Web version of this article.)

chromatography (HPLC), that the ternary electrocatalysts favor the acetaldehyde and acetic acid formation from the EOR. For the PtSnNi/C electrocatalyst, the selectivity to only acetaldehyde can be related to dissolution process during single cell operation discussed in a previous work [43] and confirmed by EDS analysis presented in Fig. 6.

The EDS analysis was employed to compare the chemical composition of the electrocatalysts before and after DEFC tests. The Ni and Sn relative mass ratio was lower on the catalytic anodic layer of PtSnNi/C than on PtSnNi/MWCNT-COOH. For the PtSnNi/C electrocatalyst, the selectivity to only acetaldehyde can be related to Sn and Ni dissolution process under operation conditions, that can lead to the electrocatalytic activity similar to Pt/C [76], decreasing the power density gradually, as observed in Fig. 4. In contrast, the presence of Ni and Sn, with its oxide species - before and after DEFC experiments - can help the ethanol oxidation by electronic effect and bifunctional mechanisms [77,78] in the case of PtSnNi/MWCNT-COOH, resulting to diverse selectivity compared to electrocatalyst supported on carbon Vulcan® XC-72. Additionally, the presence of the functional groups in the MWCNT-COOH intensifies the metal-support interaction improving the stability of the electrocatalyst as observed from the superior voltage during the polarization curve (Fig. 4), a similar result was obtained in a previous work [59] using the same MWCNT-COOH, in which the PtSn/MWCNT-COOH keeping the normalized current for the EOR higher than when using Pt_3Sn_1/C E-TEK.

4. Conclusions

In this study, it was observed that the same nanoparticles preparation protocol can generate in electrocatalysts with different properties due to the utilization of different supports. The PtSnNi electrocatalysts supported on −COOH functionalized multiwalled carbon nanotubes presented a metal enrichment on surface, considerable formation of Sn oxides species, higher dilation of the Pt lattice parameter, and smaller nanoparticle size than PtSnNi/C, which presented physical characteristics very similar to Pt/C due to the opposite contribution of Ni and Sn as auxiliary metals. From the performance of a DEFC monitored by GC, the material supported on Vulcan® XC-72 carbon led to a good electrical properties in the polarization curve activation region, while the PtSnNi/MWCNT-COOH presented the same maximum power density (12 mW cm^{-2}) than PtSnNi/C and less pronounced decay of voltage at 0.1 A during 80 min. This stability can be related to two main factors: products of reaction selectivity and modification of chemical composition (metal dissolution) of the electrocatalysts. While PtSnNi/MWCNT-COOH presented selectivity for acetic acid and acetaldehyde, the electrocatalyst supported on Vulcan® XC-72 produced only acetaldehyde. In addition, by EDS, it was indicated higher dissolution of the Sn and Ni in PtSnNi/C from the more intense diminution of their relative chemical contribution comparing to electrocatalyst supported on MWCNT−COOH. Hence, our results indicate that PtSnNi/MWCNT-COOH represents a promising electrocatalyst for the anode in DEFCs.

Acknowledgments

The authors are grateful to the Multiuser Central Facilities (UFABC) and Laboratório Nacional de Luz Síncroton (LNLS). This work was supported by CNPq (process number: 429727/2018-6) and FAPESP projects and fellowships (process numbers 2011/00008-2, 2015/21366-9, 2015/26308-7, 2016/00819-8, 2017/21846-6, 2017/10118-0). P.H.C.C and M.C.S. thank the CNPq for the research fellowships.

Appendix A. Supplementary data

Supplementary data to this article can be found online at https://doi.org/10.1016/j.renene.2019.05.067.

References

[1] S. Chauhan, T. Mori, T. Masuda, S. Ueda, G.J. Richards, J.P. Hill, K. Ariga, N. Isaka, G. Auchterlonie, J. Drennan, Design of low Pt concentration electrocatalyst surfaces with high oxygen reduction reaction activity promoted by formation of a heterogeneous interface between Pt and CeOx nanowire, ACS Appl. Mater. Interfaces 8 (14) (2016) 9059–9070.
[2] S.T. Hunt, M. Milina, Z. Wang, Y. Román-Leshkov, Activating earth-abundant electrocatalysts for efficient, low-cost hydrogen evolution/oxidation: sub-monolayer platinum coatings on titanium tungsten carbide nanoparticles, Energy Environ. Sci. 9 (2016) 3290–3301.
[3] E.V. Spinacé, A.O. Neto, M. Linardi, Electro-oxidation of methanol and ethanol using PtRu/C electrocatalysts prepared by spontaneous deposition of platinum on carbon-supported ruthenium nanoparticles, J. Power Sources 129 (2004) 121–126.
[4] C.G. Lee, M. Umeda, I. Uchida, Cyclic voltammetric analysis of C1-C4 alcohol electrooxidations with Pt/C and Pt-Ru/C microporous electrodes, J. Power Sources 160 (2006) 78–89.
[5] Available in: http://platinumprice.org/platinum-price-per-kilo.html.Acessado em:Outubro/2015.
[6] M.J. Janik, M. Neurock, A first-principles analysis of electro-oxidation of CO over. Pt (111), Electrochim. Acta 52 (2007) 5517–5528.
[7] A. Brouzgou, S.Q. Song, P. Tsiakaras, Low and non-platinum electrocatalysts for PEMFCs: current status, challenges and prospects, Appl. Catal. B Environ. 127 (2012) 371–388.
[8] H. Wendt, E.V. Spinacé, A.O. Neto, M. Linardi, Electrocatalysis and electrocatalysts for low temperature fuel cells: fundamentals, state of the art, research and development, Quím. Nova 28 (2005) 1066–1075.
[9] W.J. Zhou, W.Z. Li, S.Q. Song, Z.H. Zhou, L.H. Jiang, G.Q. Sun, Q. Xin, K. Poulianitis, S. Kontou, P. Tsiakaras, Bi- and tri-metallic Pt based anode catalysts for direct ethanol fuel cells, J. Power Sources 131 (2004) 217–223.
[10] A.O. Neto, R.R. Dias, M.M. Tusi, M. Linard, E.V. Spinacé, Electro- oxidation of methanol and ethanol using PtRu/C, PtSn/C and PtSnRu/C electrocatalysts prepared by an alcohol-reduction process, J. Power Sources 166 (2007) 87–91.
[11] R.T.S. Oliveira, M.C. Santos, B.G. Marcussi, P.A.P. Nascente, L.O.S. Bulhões, E.C. Pereira, The use of metallic bilayer for the oxidation of small organic molecules, J. Electroanal. Chem. 575 (2005) 177–182.
[12] S. Song, P. Tsiakaras, Recent progress in direct ethanol proton exchange membrane fuel cells (DE-PEMFCs), Appl. Catal. B Environ. 63 (2006) 187–193.
[13] X. Xue, J. Ge, T. Tian, C. Liu, W. Xing, T. Lu, Enhancement of the electro-oxidation of ethanol on Pt–Sn–P/C catalysts prepared by chemical deposition process, J. Power Sources 172 (2007) 560–569.
[14] F. Vigier, C. Coutanceau, F. Hahn, E.M. Belgsir, C. Lamy, On the mechanism of ethanol electro-oxidation on Pt and PtSn catalysts: electrochemical and in situ IR reflectance spectroscopy studies, J. Electroanal. Chem. 563 (2004) 81–89.
[15] J. Ribeiro, D.M. Dos Anjos, J.M. Leger, F. Hahn, P. Olivi, A.R. Andrade, G. Tremiliosi-Filho, K.B. Kokoh, J. Appl. Eletrochem. 38 (2008) 653–662.
[16] E. Antolini, Catalysts for direct ethanol fuel cells, J. Power Sources 170 (2007) 1–12.
[17] T.S. Almeida, L.M. Palma, P.H. Leonello, C. Morais, K.B. Kokoh, A.R. De Andrade, An optimization study of PtSn/C catalysts applied to direct ethanol fuel cell: effect of the preparation method on the electrocatalytic activity of the catalysts, J. Power Sources 215 (53–62) (2012).
[18] E. Antolini, F. Colmati, E.R. Gonzalez, Effect of Ru addition on the structural characteristics and the electrochemical activity for ethanol oxidation of carbon supported Pt–Sn alloy catalysts, Electrochem. Commun. 9 (2007) 398–404.
[19] E. Ribadeneira, B.A. Hoyos, Evaluation of Pt–Ru–Ni and Pt–Sn–Ni catalysts as anodes in direct ethanol fuel cell, J. Power Sources 180 (2008) 238–242.
[20] E.V. Spinacé, M. Linardi, A.O. Neto, Co-catalytic effect of nickel in the electro-oxidation of ethanol on binary Pt-Sn electrocatalysts, Electrochem. Commun. 7 (2005) 365–369.
[21] A. Bonesi, G. Garaventa, W.E. Triaca, A.M. Castro Luna, Synthesis and characterization of new electrocatalysts for ethanol oxidation, Int. J. Hydrogen Energy 33 (2008) 3499–3501.
[22] A.O. Neto, L.A. Farias, R.R. Dias, M. Brandalise, M. Linardi, E.V. Spinacé, Enhanced electro-oxidation of ethanol using PtSn/CeO_2–C electrocatalyst prepared by an alcohol-reduction process, Electrochem. Commun. 10 (2008) 1315–1317.
[23] M. Wang, Y. He, R. Li, Z. Ma, Z. Zhang, X. Wang, Electrochemical activated PtAuCu alloy nanoparticle catalysts for formic acid, methanol and ethanol electro-oxidation, Electrochim. Acta 178 (2015) 259–269.
[24] X. Wang, F. Zhu, Y. He, M. Wang, Z. Zhang, Z. Ma, R. Li, Highly active carbon supported ternary PdSnPtx (x=0.1~0.7) catalysts for ethanol electro-oxidation in alkaline and acid media, J. Colloid Interface Sci. 468 (2016) 200–210.
[25] B. Habibi, E. Dadashpour, Carbon-ceramic supported bimetallic Pt–Ni nanoparticles as an electrocatalyst for electrooxidation of methanol and ethanol in

acidic media, Int. J. Hydrogen Energy 38 (13) (2013) 5425–5434.
[26] K. Ding, Y. Zhao, L. Liu, Y. Cao, Q. Wang, H. Gu, X. Yan, Z. Guo, Pt–Ni bimetallic composite nanocatalysts prepared by using multi-walled carbon nanotubes as reductants for ethanoloxidation reaction, Int. J. Hydrogen Energy 39 (31) (2014) 17622–17633.
[27] D. Soundararajan, J.H. Park, K.H. Kim, J.M. Ko, Pt–Ni alloy nanoparticles supported on CNF as catalyst for direct ethanol fuel cells, Curr. Appl. Phys. 12 (3) (2012) 854–859.
[28] L. Jiang, L. Colmenares, Z. Jusys, G.Q. Sun, R.J. Behm, Ethanol electrooxidation on novel carbon supported Pt/SnOx/C catalysts with varied Pt:Sn, Electrochim. Acta 53 (2) (2007) 377–389.
[29] G.W. Huber, J.W. Shabaker, J.A. Dumesic, Raney Ni-Sn catalyst for H_2 production from biomass-derived hydrocarbons, Science 300 (2003) 2075–2077.
[30] K.-W. Park, Y.-E. Sung, M.F. Toney, Structural effect of PtRu–WO_3 alloy nanostructures on methanol electrooxidation, Electrochem. Commun. 8 (2006) 359–363.
[31] K.-S. Lee, Electrocatalytic activity and stability of Pt supported on Sb-doped SnO_2 nanoparticles for direct alcohol fuel cells, J. Catal. 258 (2008) 143–152.
[32] S. Zhang, X.-Z. Yuan, J.N.C. Hin, H. Wang, K.A. Friedrich, M. Schulze, A review of platinum-based catalyst layer degradation in proton exchange membrane fuel cells, J. Power Sources 194 (2009) 588–600.
[33] J. Wang, J. Xi, Y. Bai, Y. Shen, J. Sun, L. Chen, W. Zhu, X. Qiu, Structural designing of Pt-CeO_2/CNTs for methanol electro-oxidation, J. Power Sources 164 (2007) 555–560.
[34] M. Wang, Z. Ma, R. Li, B. Tang, X.-Q. Bao, Z. Zhang, X. Wang, Novel flower-like PdAu(Cu) anchoring on a 3D rGO-CNT sandwich-stacked framework for highly efficient methanol and ethanol electro-oxidation, Electrochim. Acta 227 (2017) 330–344.
[35] F. Zhu, G. Ma, Z. Bai, R. Hang, B. Tang, Z. Zhang, X. Wang, High activity of carbon nanotubes supported binary and ternary Pd-based catalysts for methanol, ethanol and formic acid electro-oxidation, J. Power Sources 242 (2013) 610–620.
[36] V. Mazumder, Y. Lee, S. Sun, Recent development of active nanoparticle catalysts, Adv. Funct. Mater. 20 (2010) 1224–1231.
[37] J. Guo, G. Sun, Q. Wang, G. Wang, Z. Zhou, S. Tang, L. Jiang, B. Zhou, Q. Xin, Carbon nanofibers supported Pt–Ru electrocatalysts for direct methanol fuel cells, Carbon 44 (2006) 152–157.
[38] D. Chu, Z. Li, X. Yuan, J. Li, X. Wei, Y. Wan, Electrocatalytic properties of carbon nanotubes supported ternary PtSnIn catalysts for ethanol electro-oxidation, Electrochim. Acta 78 (2012) 644–648.
[39] J.E. Thomas, A.R. Bonesi, M.S. Moreno, A. Visintin, A.M. Castro Luna, W.E. Triaca, Carbon nanotubes as catalyst supports for ethanol oxidation, Int. J. Hydrogen Energy 35 (2010) 11681–11686.
[40] Y.-C. Chiang, W.-H. Lin, Y.-C. Chang, The influence of treatment duration on multi-walled carbon nanotubes functionalized by H_2SO_4/HNO_3 oxidation, Appl. Surf. Sci. 257 (2011) 2401–2410.
[41] D.Z. Mezalira, M. Bron, High stability of low Pt loading high surface area electrocatalysts supported on functionalized carbon nanotubes, J. Power Sources 231 (2013) 113–121.
[42] Y.Y. Shao, G.P. Yin, Y.Z. Gao, P.F. Shi, Durability study of PtC and PtCNTs catalysts under simulated PEM fuel cell conditions, J. Electrochem. Soc. 153 (6) (2006) A1093–A1097.
[43] L.S. Parreira, J.C.M. da Silva, M. D'Villa –Silva, F.C. Simões, M.C. dos Santos, PtSnNi/C nanoparticle electrocatalysts for the ethanol oxidation reaction: Ni stability study, Electrochim. Acta 96 (2013) 243–252.
[44] R.M. Antoniassi, A.O. Neto, M. Linardi, E.V. Spinacé, The effect of acetaldehyde and acetic acid on the direct ethanol fuel cell performance using $PtSnO_2$/C electrocatalysts, Int. J. Hydrogen Energy 38 (27) (2013) 12069–12077.
[45] P. Chen, L.M. Chew, W. Xia, The influence of the residual growth catalyst in functionalized carbon nanotubes on supported Pt nanoparticles applied in selective olefin hydrogenation, J. Catal. 307 (2013) 84–93.
[46] W. Li, C. Liang, W. Zhou, J. Qiu, Z. Zhou, G. Sun, Q. Xin, Preparation and characterization of multiwalled carbon nanotube-supported platinum for cathode catalysts of direct methanol fuel cells, J. Phys. Chem. B 107 (2003) 6292–6299.
[47] J.F. Moulder, W.F. Stickle, P.E. Sobol, K.D. Bomben, Handbook of X-Ray Photoelectron Spectroscopy, Physical Electronics, 1995, 13: 9780964812413, (Hardcover).
[48] E.I. Vovk, A.V. Kalinkin, M.Y. Smirnov, I.O. Klembovskii, V.I. Bukhtiyarov, XPS study of stability and reactivity of oxidized Pt nanoparticles supported on TiO_2, J. Phys. Chem. C 121 (32) (2017) 17297–17304.
[49] Y. Shen, Z.H. Zhang, R.R. Long, K.J. Xiao, J.Y. Xi, Synthesis of ultrafine Pt nanoparticles stabilized by pristine graphene nanosheets for electro-oxidation of methanol, ACS Appl. Mater. Interfaces 6 (17) (2014) 15162–15170.
[50] K. Artyushkova, B. Halevi, M. Padilla, P. Atanassov, E.A. Baranova, Study of electrooxidation of ethanol on PtSn nanoparticles in alkaline and acid media, J. Electrochem. Soc. 162 (6) (2015) H345–H351.
[51] R.I. Hegde, S.R. Sainkar, S. Badrinarayanan, A.P.B. Sinha, A study of dilute tin alloys by x-ray photoelectron spectroscopy, J. Electron. Spectrosc. Relat. Phenom. 24 (1) (1981) 19–25.
[52] S. Beyhan, N.E. Sahin, S. Pronier, J.-M. Leger, F. Kadirgan, Comparison of oxygen reduction reaction on Pt/C, Pt-Sn/C, Pt-Ni/C, and Pt-Sn-Ni/C catalysts prepared by Bönnemann method: a rotating ring disk electrode study, Electrochim. Acta 151 (2015) 565–573.
[53] P.S. Correa, E.L. da Silva, R.F. da Silva, C. Radtke, B. Moreno, E. Chinarro, C.F. Malfatti, Effect of decreasing platinum amount in Pt-Sn-Ni alloys supported on carbon Mechanistic aselectrocatalysts for ethanol electrooxidation, Int. J. Hydrogen Energy 37 (2012) 9314–9323.
[54] N.M. Deraz, Effect of NiO content on structural, surface and catalytic characteristics of nano-crystalline NiO/CeO2 system, Ceram. Int. 38 (1) (2012) 747–753.
[55] S.Y. Shen, T.S. Zhao, J.B. Xu, Y.S. Li, Synthesis of PdNi catalysts for the oxidation of ethanol in alkaline direct ethanol fuel cells, J. Power Sources 195 (2010) 1001–1006.
[56] Y. Zhao, E. Yifeng, L. Fan, Y. Qiu, S. Yang, A new route for the electrodeposition of platinum–nickel alloy nanoparticles on multi-walled carbon nanotubes, Electrochim. Acta 52 (2007) 5873–5878.
[57] F. Liu, J.Y. Lee, W.J. Zhou, Segmented Pt/Ru, Pt/Ni, and Pt/RuNi nanorods as model bifunctional catalysts for methanol oxidation, Small 2 (1) (2006) 121–128.
[58] M. Arvand, M. Hassannezhad, Magnetic core–shell Fe_3O_4@SiO_2/MWCNT nanocomposite modified carbon paste electrode for amplified electrochemical sensing of uric acid, Mater. Sci. Eng. C 36 (2014) 160–167.
[59] L.S. Parreira, J.C.M. Silva, F.R. Simões, M.A.L. Cordeiro, R.H. Sato, E.R. Leite, M.C. Santos, PtSn electrocatalyst supported on MWCNT-COOH: investigating the ethanol oxidation reaction, ChemElectroChem 4 (2017) 1950–1958.
[60] A.K. Shukla, M. Neergat, P. Bera, V. Jayaram, M.S. Hegde, An XPS study on binary and ternary alloys of transition metals with platinized carbon and its bearing upon oxygen electroreduction in direct methanol fuel cells, J. Electroanal. Chem. 504 (2001) 111–119.
[61] D. Wang, S. Lu, S.P. Jiang, Tetrahydrofuran-functionalized multi-walled carbon nanotubes as effective support for Pt and PtSn electrocatalysts of fuel cells, Electrochim. Acta 55 (2010) 2964–2971.
[62] S. Beyhan, C. Coutanceau, J.-M. Léger, T.W. Napporn, F. Kadırgan, Promising anode candidates for direct ethanol fuel cell: carbon supported PtSn-based trimetallic catalysts prepared by Bönnemann method, Int. Hydrogen Energy 38 (2013) 6830–6841.
[63] A.M. Castro Luna, A.R. Bonesi, M.S. Moreno, G. Zampieri, S. Bengio, W.E. Triaca, Influence of metallic oxides on ethanol oxidation, Int. J. Hydrogen Energy 39 (2014) 8690–8696.
[64] X. Lu, W.-L. Yim, B.H.R. Suryanto, C. Zhao, Electrocatalytic oxygen evolution at surface-oxidized multiwall carbon nanotubes, J. Am. Chem. Soc. 137 (8) (2015) 2901–2907.
[65] E. Ribadeneira, B.A. Hoyos, Evaluation of Pt–Ru–Ni and Pt–Sn–Ni catalysts as anodes in direct ethanol fuel cell, J. Power Sources 180 (2008) 238–242.
[66] T.S. Almeida, A.R. Van Wassen, R.B. Van Dover, A.R. de Andrade, H.D. Abruña, Combinatorial PtSnM (M = Fe, Ni, Ru and Pd) nanoparticle catalyst library toward ethanol electrooxidation, J. Power Sources 284 (2015) 623–630.
[67] C.M. Zalitis, D. Kramer, A.R. Kucernak, Electrocatalytic performance of fuel cell reactions at low catalyst loading and high mass transport, Phys. Chem. Chem. Phys. 15 (2013) 329–4340.
[68] E.A. Ticianelli, J.G. Beery, S. Srinivasan, Dependence of performance of solid polymer electrolyte fuel cells with low platinum loading on morphologic characteristics of the electrodes, J. Appl. Electrochem. 21 (1999) 597–605.
[69] J.H. Wee, K.-Y. Lee, S.-H. Kim, Fabrication methods for low-Pt-loading electrocatalysts in proton exchange membrane fuel cell systems, J. Power Sources 165 (2007) 667–677.
[70] S. Thanasilpa, M. Hunsoma, Preparation of a high-performance Pt–Pd/C-electrocatalyst-coated membrane for ORR in PEM fuel cells via a combined process of impregnation and seeding: effect of electrocatalyst loading on carbon support, Electrochim. Acta 56 (2011) 1164–1171.
[71] M.H.M.T. Assumpção, J. Nandenha, G.S. Buzzo, J.C.M. Silva, E.V. Spinacé, A.O. Neto, R.F.B. De Souza, The effect of ethanol concentration on the direct ethanol fuel cell performance and products distribution: a study using a single fuel cell/attenuated total reflectance e Fourier transform infrared spectroscopy, J. Power Sources 253 (2014) 392–396.
[72] H. Wang, Z. Jusys, R.J. Behm, Ethanol electrooxidation on a carbon-supported Pt catalyst: reaction kinetics and product yields, J. Phys. Chem. B 108 (2004) 19413–19424.
[73] D.A. Cantane, W.F. Ambrosio, M. Chatenet, F.H.B. Lima, Electro-oxidation of ethanol on Pt/C, Rh/C, and Pt/Rh/C-based electrocatalysts investigated by on-line DEMS, J. Electroanal. Chem. 681 (2012) 56–65.
[74] J.E. Thomas, A.R. Bonesi, M.S. Moreno, A. Visintin, A.M. Castro Luna, W.E. Triaca, Carbon nanotubes as catalyst supports for ethanol oxidation, Int. J. Hydrogen Energy 35 (2010) 11681–11686.
[75] T.S. Almeida, K.B. Kokoh, A.R. De Andrade, Effect of Ni on Pt/C and PtSn/C prepared by the Pechini method, Int. J. Hydrogen Energy 36 (2011) 3803–3810.
[76] S.O. Klemm, A.A. Topalov, C.A. Laska, K.J.J. Mayrhofer, Coupling of a high throughput microelectrochemical cell with online multielemental trace analysis by ICP-MS, Electrochem. Commun. 13 (2011) 1533–1535.
[77] K. Artyushkova, B. Halevi, M. Padilla, P. Atanassov, E.A. Baranova, Mechanistic study of electrooxidation of ethanol on PtSn nanoparticles in alkaline and acid media, J. Electrochem. Soc. 162 (6) (2015) H345–H351.
[78] J.E. Sulaiman, S. Zhu, Z. Xing, Q. Chang, M. Shao, Pt–Ni octahedra as electrocatalysts for the ethanol electro-oxidation reaction, ACS Catal. 7 (2017) 5134–5141.